Spin Dynamics II: Damping William Rippard, Chairman

Dependence of anisotropy and damping on shape and aspect ratio in micron sized $Ni_{81}Fe_{19}$ elements

A. Barman, V. V. Kruglyak, and R. J. Hicken
School of Physics, University of Exeter, Stocker Road, Exeter EX4 4QL, United Kingdom

J. Scott, A. Kundrotaite, and M. Rahman
Department of Physics and Astronomy, University of Glasgow, Glasgow G12 8QQ, United Kingdom

(Presented on 8 January 2004)

We have studied magnetic anisotropy and damping in $Ni_{81}Fe_{19}$ elements of different shape and aspect ratio by time-resolved scanning Kerr effect microscopy and micromagnetic simulations. Square elements show a fourfold anisotropy that becomes weaker with increasing aspect ratio. Square elements with aspect ratio <230 show an anisotropy of the apparent damping that becomes stronger with decreasing aspect ratio. Variations in the apparent damping may be understood in terms of dephasing of spin wave modes that leads to the appearance of fringes in time-resolved magnetic images. © *2004 American Institute of Physics.* [DOI: 10.1063/1.1687273]

Recent developments in magnetic storage technology require precessional switching to be achieved and understood in micrometer and nanometer sized elements. A few attempts have been made to understand the spatial uniformity of precessional switching and small amplitude magnetization dynamics.[1–4] These revealed that nonuniform precessional dynamics occur due to spin wave generation, and an anisotropy in the apparent damping was observed at the center of a square $Ni_{81}Fe_{19}$ element.[4] The latter effect occurs because the nature of the mode spectrum changes as the orientation of the static field is varied, leading to different dephasing behavior. In a rectangular element the presence of a fourfold configurational anisotropy has been known for some time.[5,6] This is associated with the gradual variation of the initial magnetization from a ''flower state'' to a ''leaf state'' as the applied magnetic field is rotated from an edge towards a diagonal of the rectangle. A fourfold anisotropy has been observed by various techniques[4–6] and is believed to depend upon the aspect (width/thickness) ratio of the measured element.[5,6] Here, we have employed time-resolved scanning Kerr effect microscopy to study the dependence of the configurational anisotropy and apparent damping upon the shape and aspect ratio. The time-dependent Kerr rotation may be used to investigate the damping and detect the presence of nonuniform resonant modes. Time-resolved images provide a means by which to visualize the spatial nature of the modes and understand the underlying mechanism of the apparent damping. Micromagnetic simulations have been used to understand the experimental results.

A series of square $Ni_{81}Fe_{19}$ elements and one circular $Ni_{81}Fe_{19}$ element were studied. The circle (S1, aspect ratio $=67$) and the first square (S2, aspect ratio$=67$) had 10 μm width and 150 nm thickness, while the other three squares had widths of 10 μm (S3, aspect ratio$=454$), 7 μm (S4, aspect ratio$=318$), and 5 μm (S5, aspect ratio$=227$) and 22 nm thickness. Pump-probe measurements were performed with a time-resolved scanning Kerr effect microscope[7] at a wavelength of 790 nm. The instantaneous out of plane magnetization component was probed by means of the polar magneto-optical Kerr effect. A pulsed field with 40 ps rise time and peak amplitude of about 30 Oe (S1 and S2) or 40 Oe (S3–S5) was generated by a photoconductive switch and delivered to the sample by either a coplanar stripline or a coplanar waveguide structure made from Au on GaAs. Samples S1 and S2 were fabricated on glass substrates and placed face down on a coplanar stripline with track width and separation of 30 μm so as to experience an in-plane pulsed field while being probed through the glass substrate. Samples S3–S5 were deposited directly onto the 12 μm wide central conductor of a coplanar waveguide structure with a 9 μm track separation. $Ni_{81}Fe_{19}$ was deposited either by sputtering (S1, S2) from a base pressure of 2×10^{-7} Torr or by evaporation (S3–S5) at a base pressure of 2×10^{-6} Torr onto a bilayer of patterned polymethylmethacrylate (PMMA) resist. Samples S1 and S2 were capped by a 20 nm thick layer of Al_2O_3 while samples S3–S5 were left uncapped. The probe was focused to a submicron spot using a microscope objective with (numerical aperture) NA$=0.65$ and the sample was scanned under the probe spot to acquire time-resolved images. A static field **H** of strength H and orientation ϕ_H was applied in the sample plane.

Figure 1 shows typical measured time-dependent Kerr rotations when the probe beam was focused at the center of each element. Scans are shown for $\phi_H=90°$ and 45° in each panel. Measurements were performed in the field range $100<H\leqslant500$ Oe during which no significant variation of the anisotropy field and apparent damping for a particular sample was observed. Fast Fourier transform (FFT) power

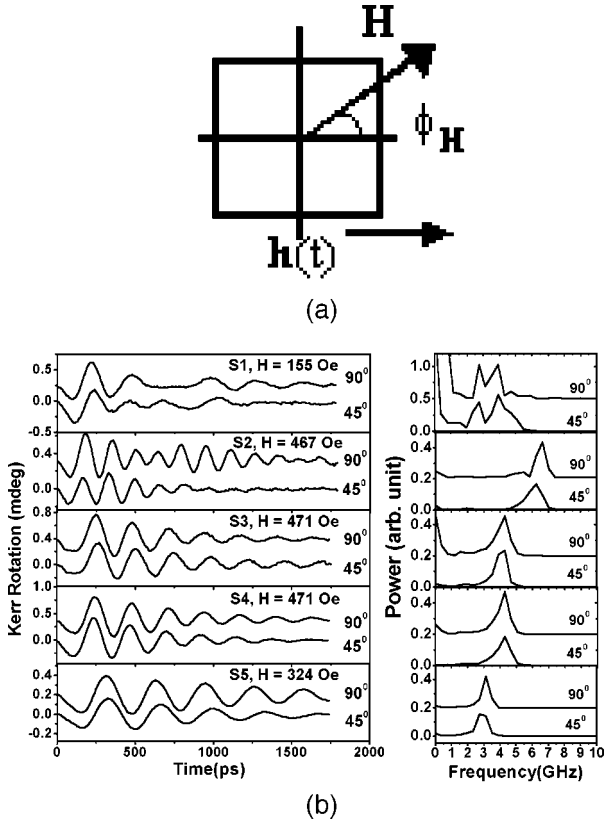

FIG. 1. (a) The experimental geometry is shown. (b) The measured time-dependent Kerr rotations are shown for samples S1–S5 at $\phi_H = 90°$ and 45°. The right hand panels show the corresponding FFT spectra.

spectra were calculated from each time scan using a Welch window function. The mode frequency was taken as the median of the half-height frequencies is plotted against ϕ_H in Fig. 2. Samples S2–S5 show a superposition of a fourfold, twofold, and onefold variation with ϕ_H, with the fourfold variation becoming weaker as the aspect ratio of the square element increases. For S1 there is apparently no fourfold variation but a twofold and a onefold variation are still observed. The frequency vs ϕ_H data have been modeled by

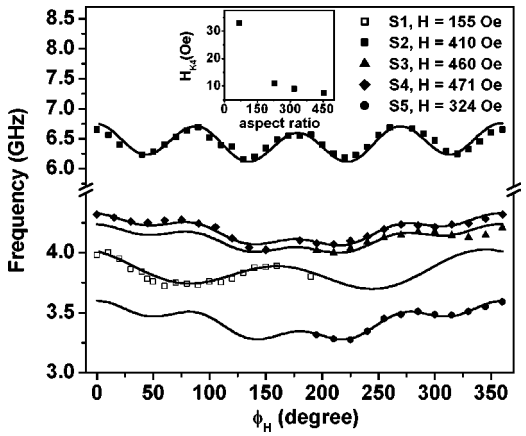

FIG. 2. Experimental (points) and simulated (curves) frequencies are plotted as a function of the angle ϕ_H. The experimental geometry is as shown in Fig. 1(a). The inset shows the variation of the fourfold anisotropy field (H_{K4}) with aspect ratio.

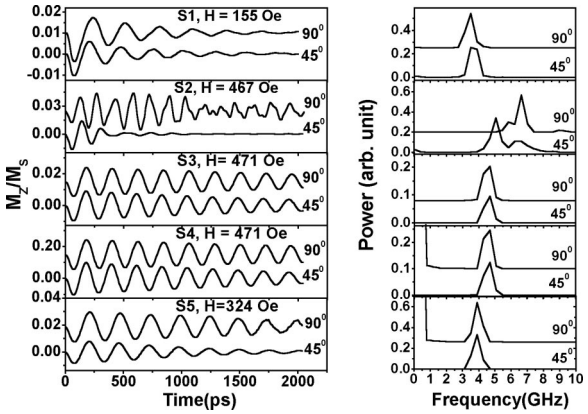

FIG. 3. The simulated out of plane component of magnetization is shown for samples S1, S2, S3, S4, and S5 for $\phi_H = 90°$ and 45°. The right hand panels show the corresponding FFT power spectra.

solving the Landau-Lifshitz equation in the macrospin limit.[4] The changing orientation of the time averaged pulsed field relative to **H** is responsible for the onefold variation of the frequency with ϕ_H.[4] The simulated frequencies are shown as the solid curves in Fig. 2. The values of the twofold uniaxial anisotropy field were found to be about 2–3 Oe for the square elements and about 8 Oe for the circular element. The values of the fourfold anisotropy field (H_{K4}) were 33 Oe for S2, 7.5 Oe for S3, 9 Oe for S4, and 11 Oe for S5 as shown in the inset in Fig. 2. The easy axes of the fourfold anisotropy were parallel to the edges of the element. The decrease in the fourfold anisotropy field with increasing aspect ratio is in agreement with a previous report.[6] The values of the g factor and $4\pi M$ demagnetizing field used in the simulations were 2.1 and 10.8 kOe, respectively, for S1 and S2, and 2.0 and 5.7 kOe, respectively, for S3–S5. The reduction of $4\pi M$ for the uncapped thinner samples may be the result of either partial oxidation or a deviation from the intended alloy composition. However we do not expect this to affect our conclusions about the influence of the shape and aspect ratio upon the configurational anisotropy and variations in the apparent damping within a particular element.

Comparing $\phi_H = 90°$ and 45°, S1 shows almost no difference in the apparent damping while S2 shows a clear anisotropy, suggesting that the effect is related to the shape of the element. However to investigate whether the aspect ratio of a square element has any influence, we consider the time-dependent Kerr rotation obtained from each square element. S3 and S4 (aspect ratio 454 and 318) show no significant anisotropy, S5 (aspect ratio = 227) shows a small anisotropy which then becomes much stronger in S2 (aspect ratio = 67).

Micromagnetic simulations were performed with the OOMMF software,[8] using the parameter values deduced from the data shown in Fig. 2. The elements were divided into two-dimensional square cells with width varying from 10 nm to 40 nm. The simulations were performed with a pulsed field of 40 ps rise time while the magnitudes of the static and pulsed fields were similar to those used in the experiment. The simulated response was found to lie in the linear regime in all cases. The time-dependent magnetization was spatially

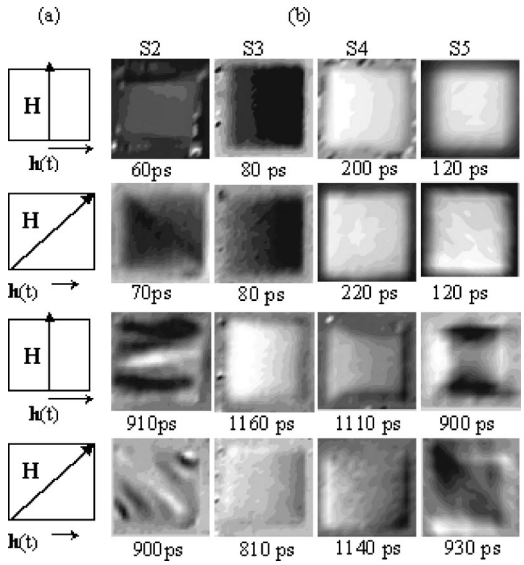

FIG. 4. The time-resolved Kerr images (b) obtained in the geometries (a) are shown for S2, H=155 Oe; S3, H=471 Oe; S4, H=471 Oe; and S5, H=324 Oe. The delay times are shown under each image.

averaged over a 0.8 μm square mask, of comparable area to that of the focused probe spot, placed at the center of the element. Figure 3 shows the time dependence of the out of plane component of the magnetization for $\phi_H=90°$ and 45°. A significant anisotropy in the apparent damping is observed for S2 and S5 but not for S1, S3, and S4, demonstrating that the anisotropy in the apparent damping increases with decreasing aspect ratio, as observed in the experiment. For S3–S5 the apparent damping in the measurement is generally greater than that in the simulation. This suggests that the mechanism responsible for the reduced value of $4\pi M$ also leads to an increase in the intrinsic damping.

Time-resolved images of the magnetization were acquired to understand why the damping appears to be anisotropic, and how it depends on aspect ratio in square elements. Experimental images from S2, S3, S4, and S5 are shown in Figs. 4(b–e). The gray scale represents the out of plane component of magnetization. Figure 4(b) shows the presence of nonuniformity in S2 in both geometries but fringes appear from different regions and their distribution is different in the two geometries. The anisotropy in the apparent damping in this sample can be understood in terms of dephasing of confined magnetostatic spin wave modes with wave vector parallel to the static field. For S3 the precessional motion is spatially uniform for both geometries while for S4 small nonuniform regions appear at the edges and the corners for $\phi_H=90°$ and 45°, respectively, leaving the central part of the sample spatially uniform. The images for S5 show fringes that are well defined but fewer than in S2. The number of fringes observed within a particular element indicates the extent of the dephasing of the excited modes. Assuming that the wavelengths of the allowed modes scale with the length of the element, and that their frequency depends upon the ratio of the wavelength to the thickness of the element,[9] then the difference in frequency of successive modes, and hence the dephasing time, would be expected to depend upon the aspect ratio of the element as we observe.

In conclusion we have investigated the dependence of fourfold magnetic anisotropy and an anisotropy of the apparent damping upon shape and aspect ratio in micron sized $Ni_{81}Fe_{19}$ elements. The circular element showed no fourfold anisotropy or anisotropic damping, while all the square elements showed fourfold anisotropy and in some cases also an anisotropic damping. The fourfold anisotropy field and the anisotropy in the apparent damping increase with decreasing aspect ratio. The anisotropy in the apparent damping increases with the number of fringes observed within the element. The number of fringes is related to the time taken for the excited mode spectrum to dephase which is in turn determined by the aspect ratio of the element.

We gratefully acknowledge the financial support of the UK Engineering and Physical Sciences Research Council.

[1] W. K. Hiebert, G. E. Ballentine, and M. R. Freeman, Phys. Rev. B **65**, 140404 (2002).
[2] Th. Gerrits, H. A. M. van den Berg, J. Hohlfeld, L. Bar, and Th. Rasing, Nature (London) **418**, 509 (2002).
[3] J. P. Park, P. Eames, D. M. Engebretson, J. Berezovsky, and P. A. Crowell, Phys. Rev. Lett. **89**, 277201 (2002).
[4] A. Barman, V. V. Kruglyak, R. J. Hicken, A. Kundrotaite, and M. Rahman, Appl. Phys. Lett. **82**, 3065 (2003).
[5] R. P. Cowburn, A. O. Adeyeye, and M. E. Welland, Phys. Rev. Lett. **81**, 5414 (1998).
[6] S. M. Cherif, Y. Roussigne, C. Dugautier, and P. Moch, J. Magn. Magn. Mater. **242-245**, 591 (2002).
[7] A. Barman, V. V. Kruglyak, R. J. Hicken, A. Kundrotaite, and M. Rahman, IEE Proc.: Sci., Meas. Technol. **150**, 260 (2003).
[8] M. Donahue and D. G. Porter, OOMMF User's Guide, Version 1.0, URL: http://math.nist.gov/oommf
[9] R. W. Damon and J. R. Eshbach, J. Phys. Chem. Solids **19**, 308 (1961).